

1 **Infrared spectroscopy coupled with a dispersion model for quantifying the**
2 **real-time dynamics of kanamycin resistance in artificial microbiota**

3 Naifu Jin¹, Maria Paraskeva², Kirk T. Semple¹, Francis L. Martin^{2,*}, Dayi Zhang^{1,*}

4 ¹Lancaster Environment Centre, Lancaster University, Lancaster, LA1 4YQ, UK;

5 ²School of Pharmacy and Biomedical Sciences, University of Central Lancashire,
6 Preston PR1 2HE, UK

7

8

9

10

11

12

13 **Corresponding authors:*

14 Dayi Zhang, Lancaster Environment Centre, Lancaster University, Lancaster LA1
15 4YQ, UK; Tel.: +44(0)1524 510288; Fax: +44(0)1524 510082, Email:

16 d.zhang@lancaster.ac.uk

17 Francis L. Martin, School of Pharmacy and Biomedical Sciences, University of
18 Central Lancashire, Preston PR1 2HE, UK; Tel.: +44(0)1772 896482; Email:

19 flmartin@uclan.ac.uk

20

21 **Abstract**

22 Over-usage of antibiotics leads to the widespread induction of antibiotic resistance
23 genes (ARGs). Developing an approach to allow real-time monitoring and fast
24 prediction of ARGs dynamics in clinical or environmental samples has become an
25 urgent matter. Vibrational spectroscopy is potentially an ideal technique towards the
26 characterization of the microbial composition of microbiota as it is non-destructive,
27 high-throughput and label-free. Herein, we employed attenuated total reflection
28 Fourier-transform infrared (ATR-FTIR) spectroscopy and developed a
29 spectrochemical tool to quantify the static and dynamic composition of kanamycin
30 resistance in artificial microbiota to evaluate microbial antibiotic resistance. Second
31 order differentiation was introduced in identifying the spectral biomarkers, and
32 principal component analysis followed by linear discriminant analysis (PCA-LDA)
33 was used for the multivariate analysis of the entire spectral features employed. The
34 calculated results of the mathematical dispersion model coupled with PCA-LDA
35 showed high similarity to the designed microbiota structure, with no significant
36 difference ($P > 0.05$) in the static treatments. Moreover, our model successfully
37 predicted the dynamics of kanamycin resistance within artificial microbiota under
38 kanamycin pressures. This work lends new insights into the potential role of
39 spectrochemical analyses in investigating the existence and trends of antibiotic
40 resistance in microbiota.

41

42 **Keywords** Antibiotic resistance, Artificial microbiota, ATR-FTIR spectroscopy,
43 Kanamycin, Multivariate analysis, Spectrochemical

44

45 **Introduction**

46 Antibiotics have played a vital role in modern medicine contributing to a considerable
47 reduction in childhood mortality and increasing life expectancy¹. However, the
48 increasing number of fatal infections caused by antibiotic-resistant bacteria is
49 gradually developing into a global threat. The environment has become the primary
50 “sink” for most applied antibiotics and their residues arising from human or animal
51 excretion¹⁻³. Since bacteria with antibiotic resistance genes (ARGs) can tolerate
52 antibiotics, selection pressures from contaminated water or soil will boost the
53 abundance of ARGs in the environment and increase the possibility of their spread
54 through microbial species^{4,5}. Therefore, real-time monitoring and quantification of
55 ARGs or antibiotic-resistant bacteria is urgently required.

56 Besides measuring the concentration of antibiotics *via* chemical analysis, various
57 biological analytical methods have been used to determine the presence, abundance
58 and diversity of ARGs in the microbiota to capture a “static map” of their existence,
59 *e.g.*, meta-sequence and quantitative polymerase chain reaction (qPCR)^{6,7}. However,
60 genetically identical cells from the same population have stochasticity in gene
61 expression, meaning that there is significant variation in their molecular content and
62 phenotype, even under similar environmental influences. Moreover, bacterial
63 resistance to the antibiotics can also be affected and regulated epigenetically⁸. In
64 combination, these factors provide an opportunity for phenotypic and cell-type
65 diversity regardless of genotype⁹. This questions the reliability of determining ARGs
66 abundance by molecular biological approaches in real-world situations, leading to the
67 necessity of developing a phenotypic assay that depicts *in situ* dynamics of ARGs or
68 microbial antibiotic resistance in environmental samples.

69 It is well accepted that genetic and epigenetic factors cannot be studied
70 independently as a complete phenotype emerges from both together¹⁰. The
71 spectrochemical analysis is an alternative approach to characterize the phenotypic
72 features of organisms and has already demonstrated its ability to investigate clinical

73 samples, as well as to describe and identify bacterial species^{11,12}. Previous studies
74 indicates that spectroscopic techniques are capable of studying phenotypic features, at
75 either population¹³ or single-cell¹⁴ level, such as diagnosing the distinct spectral
76 signatures and metabolomes from isogenic cell lines¹⁵. However, the current
77 techniques have limited application in characterizing ARGs under antibiotic pressures,
78 mainly due to the lack of appropriate analytical models and well-trained databases.
79 Recently, some studies using spectroscopic techniques have set out to investigate
80 biological response to environmental stress, like nanomaterials^{16,17} and antimicrobial
81 reagents^{18,19}. The introduction of spectroscopic techniques coupled with a suitable
82 prediction model to characterize microbial composition may bring new insights in
83 detecting the presence or even the dynamics of microbial antibiotic resistance in
84 environmental microbiota in real-time, owing to its non-destructive, high-throughput
85 and label-free character^{20,21}. It also allows for *in situ* spectral measurements, helping
86 in understanding the interactions between microbes and their physical environment.

87 Kanamycin is a subclass of aminoglycoside antibiotics, one of the most widely
88 applied antibiotics in health and molecular biology²². Because of the well-established
89 mechanisms of kanamycin resistance and characterized sequence²³, it was selected as
90 the model antibiotic in the present study. Herein, we used attenuated total reflection
91 Fourier-transform infrared (ATR-FTIR) spectroscopy, coupled with the multivariate
92 analysis and the dispersion indicator model, to quantify the kanamycin resistance
93 within artificial microbiota and evaluate their phenotypic change associated with
94 kanamycin resistance, from both static and dynamic perspectives. This work raises the
95 potential feasibility of applying spectroscopic techniques to diagnose ARGs
96 phenotypic dynamics in the microbial community *in situ*.

97

98 **Experimental section**

99 *Sample preparation*

100 The present study included two strains without kanamycin-resistant-gene,
101 *Mycobacterium vanbaalenii* PYR-1 and *Escherichia coli* DH5 α , and one

102 kanamycin-resistant strain *Acinetobacter baylyi* ADPWH_recA, which has a
 103 continuously expressed kanamycin resistance gene *kan^R* (from Mini-Tn5/Km²⁴,
 104 Genbank accession number: U32991.1) inserted into the *recA* gene in the
 105 chromosome of *A. baylyi* ADP1²⁵. Before the experiment, they were all cultured in
 106 Luria-Bertani (LB) broth medium for 24 h at 30±2°C.

107 The three control groups contained pure *M. vanbaalenii* PYR-1, *E. coli* DH5α
 108 and *A. baylyi* ADPWH_recA, respectively. The artificial microbiotas were prepared
 109 for both static (M1 to M5) and dynamic (AM1 and AM2) experiments by gently
 110 mixing the cells in the compositions listed in Table 1. The optical density at 600 nm
 111 (OD₆₀₀) in each treatment was monitored continuously for 24 h by a multimode plate
 112 reader (FLUOstar Omega, Germany) to evaluate bacterial growth. For static tests, the
 113 cells were directly collected by centrifugation (4000 rpm for 5 min), washed three
 114 times with sterile deionized water to remove the residues of growth media and then
 115 suspended in 70% ethanol to fix the bacterial cells. For dynamic tests, all the artificial
 116 microbiotas were treated with kanamycin (final concentration 10 mg/L). After
 117 exposure for 4, 8, 12 or 24 h, the cells from microbiotas were harvested following the
 118 same procedure as above.

119

120 **Table 1.** The compositions of artificial microbiotas (volume ratio, v:v:v).

Treatments	Control			Static test					Dynamic test	
	<i>M. vanbaalenii</i>	<i>E. coli</i>	<i>A. baylyi</i>	M ₁	M ₂	M ₃	M ₄	M ₅	AM ₁	AM ₂
<i>M. vanbaalenii</i>	100%	-	-	40%	30%	30%	15%	5%	40%	25%
<i>E. coli</i>	-	100%	-	50%	45%	20%	10%	5%	40%	25%
<i>A. baylyi</i>	-	-	100%	10%	25%	50%	75%	90%	20%	50%

121

122 *ATR-FTIR spectroscopy*

123 The washed cell pellets (minimal amount >5 μL) were applied onto Low-E slides for
 124 the interrogation by ATR-FTIR spectroscopy. A TENSOR 27 FTIR spectrometer
 125 (Bruker Optics Ltd., UK) equipped with a Helios ATR attachment (containing a

126 diamond internal IRE; incidence angle of the IR beam: 45°) was used. Instrument
127 parameters were set at 32 scans and spatial resolution of 8 cm⁻¹. Before the
128 measurement of a new sample, the crystal was cleaned with deionized water and
129 background readings were retaken. A total of 30 spectra were randomly acquired for
130 each treatment (3 replicates).

131 *Computational analysis*

132 The primary analysis methods employed in this study involved multivariate analysis
133 and the dispersion indicator model. The initial data generated from ATR-FTIR
134 spectroscopy were analyzed within MATLAB R2011a (*The Maths Works, Natick, MA,*
135 *USA*) software, coupled with IRootLab toolbox (<http://irootlab.googlecode.com>)²⁶.
136 Unless otherwise stated, the acquired spectra were cut to the biochemical-cell
137 fingerprint region (1800-900 cm⁻¹), rubberband baseline corrected and normalized to
138 Amide I (1650 cm⁻¹). Second order differentiation baseline correction and vector
139 normalization was also performed as an alternative mean to process the data (the
140 number of the filter coefficients of the Savitzky-Golay smoothing/differentiation filter
141 was 9). Principal component analysis followed by linear discriminant analysis
142 (PCA-LDA) was subsequently applied to the pre-processed data to reduce the number
143 of spectra to 10 uncorrelated principal components (PCs), which account for >99% of
144 the total variance; LDA is a supervised technique coupled with PCA in order to
145 maximize inter-class and minimize intra-class variance²¹. In addition, cluster vector
146 approach was conducted to visualise the discriminating difference^{21,27}. This method
147 takes input from PCA-LDA to create a loadings vector for each category contributing
148 to respective data points. The pseudo-spectra allow identifying which variables (or
149 wavenumber) are responsible for variance in the data set related to the original
150 spectra^{21,27}. The detailed information of the dispersion indicator model was described
151 in the Electronic Supplementary Information (ESI).

152 *Biological analysis*

153 The copy numbers of total bacterial 16S rRNA and targeted kanamycin resistance
154 gene (*kan^R*) were determined by quantitative polymerase chain reaction (qPCR). For
155 16S rRNA, the primer pair set was 341F (5'-CCTACGGGNGGCWGCAG-3') and
156 805R (5'-GACTACHVGGGTATCTAATCC-3'), and the primer pair for *kan^R* was
157 KanF (5'-TGTCATAACCACTTGTCGCC-3') and KanR

158 (5'-ATCGAGCTGTATGCGGAGTG-3'). The 20 μ L qPCR system consisted of 2 μ L
159 of each primer, 1 μ L DNA template, 5 μ L molecular water and 10 μ L iTaq™
160 Universal SYBR® Green Supermix (BioRad, USA). The relative abundance of *kanR*
161 in each pure strain was calculated as the ratio of *kanR* copy numbers to 16S rRNA
162 copy numbers (*kanR*/16S). The microbial kanamycin resistance within the artificial
163 microbiota was calculated as the ratio of *A. baylyi* population to the total bacterial
164 population.

165 *Statistical analysis*

166 One-way analysis of variance (ANOVA) with Tukey's post hoc test/or T-test was
167 employed to examine the discriminating differences. All statistical analysis was
168 carried out in GraphPad Prism 6.

169

170 **Results and Discussion**

171 *Growth and kanamycin resistance gene of individual strains*

172 All the three bacterial strains (*A. baylyi* ADPWH_recA, *M. vanbaalenii* PYR-1 and *E.*
173 *coli* DH5 α) had similar growth curves without kanamycin pressure (see ESI Figure
174 S1A). Cultivated in 10 mg/L kanamycin, only *A. baylyi* ADPWH_recA maintained
175 positive growth because of the expression of *kan^R* gene and resistance to kanamycin
176 (see ESI, Figure S1B). Neither *M. vanbaalenii* PYR-1 nor *E. coli* DH5 α grew
177 post-exposure to 10 mg/L kanamycin. The results of qPCR further confirmed that the
178 high relative abundance of *kan^R* gene (*kanR*/16S) were only found in *A. baylyi*
179 ADPWH_recA (0.306 in medium without kanamycin and 0.275 in medium with 10
180 mg/L kanamycin respectively, no significant difference), whereas it was less than
181 0.001 or below the limit of detection for *M. vanbaalenii* PYR-1 or *E. coli* DH5 α (see
182 ESI, Figure S2). It was further proved that kanamycin resistance gene is only
183 detectable in *A. baylyi* ADPWH_recA, but neither *M. vanbaalenii* PYR-1 nor *E. coli*
184 DH5 α , and the latter two cannot tolerate kanamycin pressure. The active group of
185 kanamycin, 2-deoxystreptamine, impairs bacterial protein synthesis through binding
186 to prokaryotic ribosomes 30S subunit²². The *kan^R* encoding neomycin
187 phosphotransferase is an aminoglycoside-modifying enzyme, using ATP as donor to
188 modify the hydroxyl functions of 2-deoxystreptamine and inhibit its binding to

189 ribosomes²⁸. The *kan^R* gene is therefore a reliable molecular indicator in detecting the
190 kanamycin resistance.

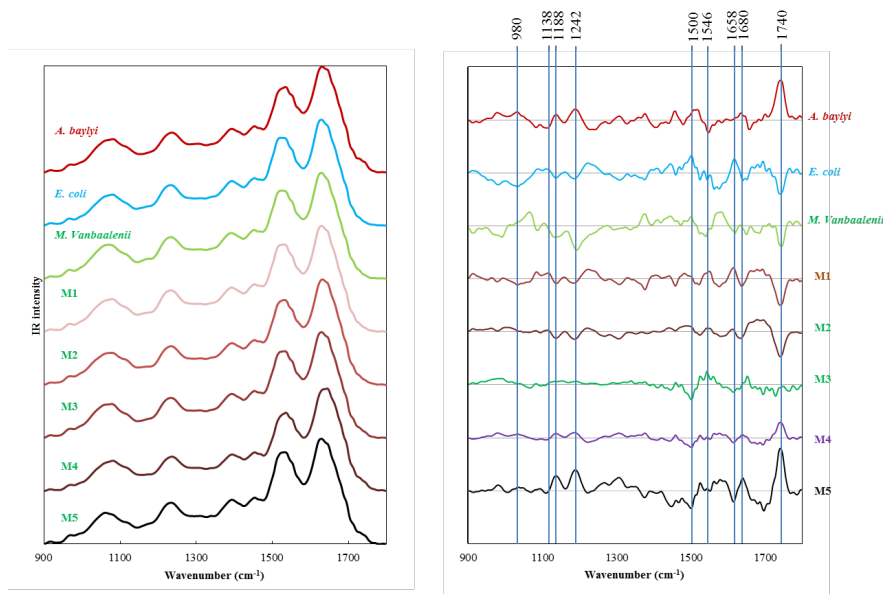
191 *IR spectral fingerprints of individual strains and microbiotas*

192 The IR spectral fingerprint region (1800 - 900 cm⁻¹) of the three strains and artificial
193 microbiotas are shown in Figure 1. The representative peaks of the biochemical
194 fingerprint include lipids (~1750 cm⁻¹), Amide I (~1650 cm⁻¹), Amide II (~1550 cm⁻¹),
195 Amide III (~1260 cm⁻¹), carbohydrate (~1155 cm⁻¹), asymmetric phosphate stretching
196 vibrations ($\nu_{as}PO_2^-$; ~1225 cm⁻¹), symmetric phosphate stretching vibrations ($\nu_sPO_2^-$;
197 ~1080 cm⁻¹), glycogen (~1030 cm⁻¹) and protein phosphorylation (~970 cm⁻¹)^{20 21}.
198 Past literatures^{12,20,29,30} suggest the characteristic peaks given by the region can be
199 used as biomarkers to characterize microbial cell types (even at subspecies level) and
200 diagnose microbe-induced diseases.

201 However, the visual spectral differences with the mean spectra are almost
202 identical regardless of the bacterial species or community composition. For this
203 reason, we applied the cluster vectors after multivariate analysis (PCA-LDA) and the
204 second order differentiation baseline correction to further reveal the underlying
205 biochemical differences between each strain or microbiota. Based on the derived
206 spectral biomarkers from PCA-LDA (Figure 1B), all the microbiota samples showed
207 marked segregation (see ESI, Table S1). Characteristics associated with microbial
208 composition were observed in particular wavenumber-absorbance intensities. For
209 instance, the intensities at 980 cm⁻¹ and 1740 cm⁻¹ were increased with increasing
210 ratio of ARGs but fluctuated in some artificial microbiotas, particularly for microbiota
211 M3 (*M. vanbaalenii* PYR-1: *E. coli* DH5 α : *A. baylyi* ADPWH_recA =
212 30%:20%:50%). Additionally, IR spectral analysis (Figure 2A) based on the second
213 order differentiation baseline correction and vector normalization highlighted several
214 key biomarkers. Two apparent shifts from ~1630 cm⁻¹ to ~1640 cm⁻¹ (Amide I) and
215 from ~1222 cm⁻¹ to ~1235 cm⁻¹ ($\nu_{as}PO_2^-$) associated with *A. baylyi* were regarded as
216 biomarkers for the presence of kanamycin resistance. These spectral alterations might
217 be attributed to the upregulated activities of the *kan^R* encoding aminoglycoside
218 *O*-phosphotransferase, which contributes to microbial resistance by inactivating
219 kanamycin molecular via catalyzing ATP-dependent phosphorylation of specific
220 aminoglycoside hydroxyl groups³¹. Some other weaker discriminations included the

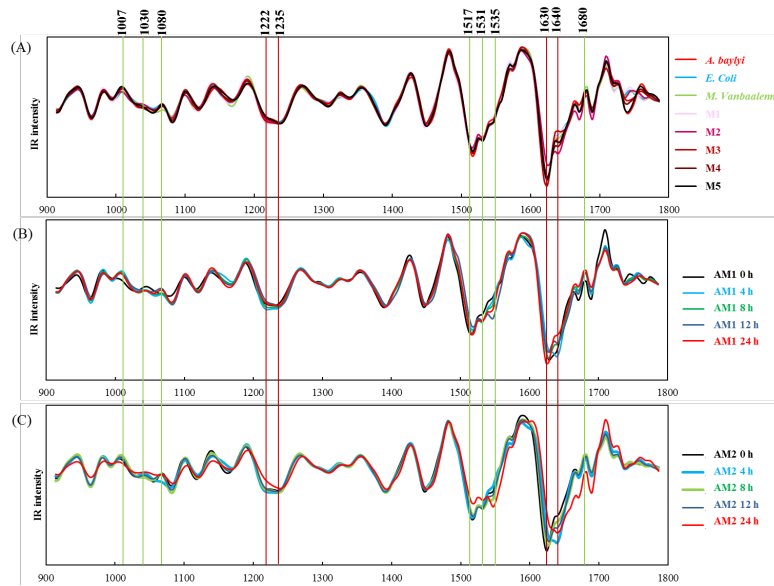
221 polysaccharide fingerprint region (1000-1150 cm^{-1}) and the protein absorbance region
222 (1500-1700 cm^{-1})²⁷. These alterations were probably induced by the interference of
223 extracellular polymeric substances (EPS) produced by different species³²⁻³⁴ and
224 resulted in the difficulties in distinguishing biomarkers from the PCA-LDA extracted
225 peaks. Based on the previous studies^{32,35,36}, we speculate that these extracellular
226 materials may interact with each other and generate new biochemical compositions
227 within the communities, influencing the discriminating peaks obtained with
228 spectrochemical interrogation.

229



230

231 **Figure 1.** (A) Infrared spectra of *A. baylyi*, *M. vanbaalenii*, *E. coli* and five artificial
232 microbiotas (M1-M5). (B) Cluster vector plots after PCA-LDA, indicating significant
233 wavenumbers for the segregation between bacterial species and artificial microbiotas.



234

235 **Figure 2.** Class means spectra of pre-processed data based on second order
 236 differentiation baseline correction and vector normalization. (A) Processed spectra of
 237 *A. baylyi*, *M. vanbaalenii*, *E. coli* and five artificial microbiotas (M1-M5). (B)
 238 Processed spectra of AM1 at different time point in dynamic experiment. (C)
 239 Processed spectra of AM1 at different time point in dynamic experiment.

240

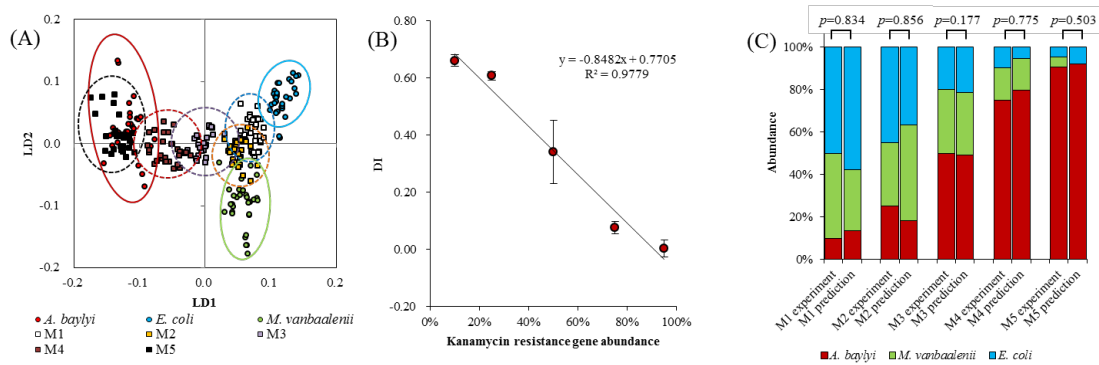
241 *Predicting community composition in artificial microbiotas*

242 Comparing to the IR spectra in the static tests, we observed identical spectral
 243 biomarkers in artificial community dynamics (Figure 2B and 2C) that the same shifts
 244 from $\sim 1630\text{ cm}^{-1}$ to $\sim 1640\text{ cm}^{-1}$ (Amide I) and from $\sim 1222\text{ cm}^{-1}$ to $\sim 1235\text{ cm}^{-1}$
 245 ($\nu_{\text{as}}\text{PO}_2^-$) developed along with the time. The results indicated the consistent spectral
 246 biomarkers in both static and dynamic microbiotas in analyzing the phenotypic
 247 presence and abundance of kanamycin resistance gene in the targeted microbiota.

248 The PCA-LDA scores plot (Figure 3A) also illustrates a significant segregation of
 249 the different groups, associated with differing microbiota compositions. The control
 250 groups (*M. vanbaalenii*, *E. coli*, and *A. baylyi*) are clearly separated from each other.
 251 In contrast to *M. vanbaalenii* and *E. coli*, all the converted spectral values of *A. baylyi*
 252 are aligned as negative along linear discriminant one (LD1), likely attributed to its
 253 kanamycin resistance. Meanwhile, along with linear discriminant two (LD2), the
 254 group of *M. vanbaalenii* (Gram-positive bacteria) is located on the negative axis alone,
 255 separated from the other two groups (*E. coli* and *A. baylyi*), which are Gram-negative.

256 The five artificial microbiota samples (M1 to M5) are located inbetween, and their
 257 distances to the control groups are correlated with their community compositions.

258



259

260 **Figure 3.** (A) Two-dimensional (LD1, LD2) scores plot after PCA-LDA of pure
 261 microbial strains and artificial microbiotas with different composition. (B) Correlation
 262 between kanamycin resistance gene abundance and group distance dispersion (D_I). (C)
 263 Comparison of artificial microbiota composition between experimental data and
 264 model prediction.

265

266 In order to predict the composition of artificial microbiota, the dispersion indicator
 267 model³⁷ was carried out by transferring the dispersion analysis from the IR spectral
 268 variables to the vectors (LD1 and LD2) and using D_I as the indicator, comparing to
 269 the ARGs gene copy numbers quantified by qPCR as reference. This method used the
 270 summarized spectral information from PCA-LDA which accounts for over 90% of
 271 spectral variations in the present study, and was more conclusive than the limited
 272 biomarkers from second order differentiation. Here, microbiotas with less abundance
 273 of *A. baylyi* were further separated from the *A. baylyi* group, but closer to those of *E.*
 274 *coli* and *M. vanbaalenii*, leading to an increasing D_I against the decreasing
 275 kanamycin resistance (kanamycin resistance genes in *A. baylyi*). Figure 3B illustrates
 276 the negative linear correlation between D_I and the abundance of *A. baylyi*
 277 (kanamycin resistance gene abundance) within the artificial microbiotas ($D_I =$
 278 $-0.8482 \times [\text{kanamycin resistance gene}] + 0.7705$). The high coefficient
 279 ($R^2=0.9779$) suggests a good linear regression of D_I against kanamycin resistance.
 280 The composition of each microbiota was, therefore, calculated from the D_I linear

281 regression based on PCA-LDA, as shown in Figure 3C. The results indicated that the
282 predicted microbial compositions had high similarity to their theoretical structure with
283 no significant differences found ($P > 0.05$). The standard deviation of microbiota M3
284 (middle point in Figure 3B) was greater than the others, possibly attributing to their
285 higher Shannon-Wiener index (1.02) than other microbiotas (0.35 to 0.94 for M1, M2,
286 M4 and M5). Shannon-Wiener index represents the diversity of microbial community,
287 and higher microbial diversity has been reported to increase complicated
288 intracommunity interaction³². It might cause huge variation of microbial chemical
289 composition, consequently leading to the difficulties in interrogating spectral
290 biomarkers and significant standard deviation in data prediction.

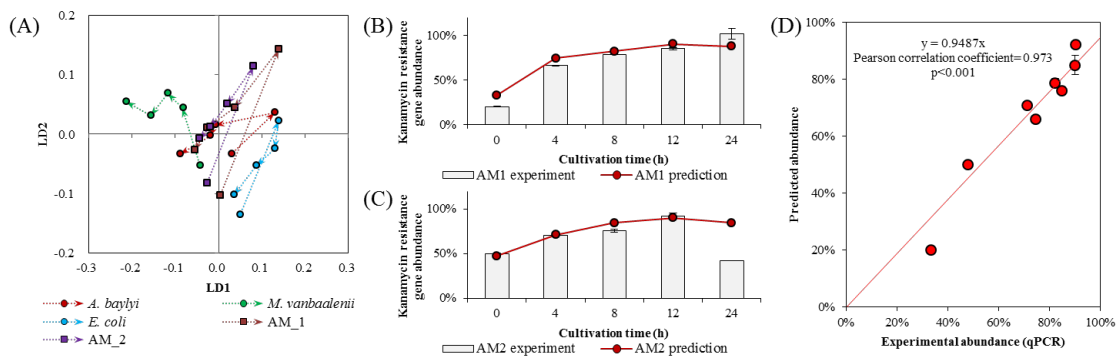
291 *Quantification of kanamycin resistance dynamics within microbiota*

292 Figure 4A illustrates the PCA-LDA scores plot of microbiotas post-exposure to
293 kanamycin, derived from the spectral dynamics of the artificial microbiotas (see ESI
294 Figure S3). All the interrogated communities exhibit a dramatic shift from the original
295 location as the exposure time increases. The *M. vanbaalenii* category moves towards a
296 different direction when compared to *A. baylyi* and *E. coli*, which might be attributed
297 to distinct cell structures between Gram-positive (*M. vanbaalenii*) and Gram-negative
298 bacteria (*A. baylyi* and *E. coli*). Specifically, there is only one lipid bilayer in the
299 membrane of Gram-positive bacteria, with a thick ring of peptidoglycan and teichoic
300 acid^{38,39}. On the other hand, the cell membrane of Gram-negative bacteria contains
301 two lipid associated bilayers, which appear to increase the chance that the applied
302 treatments influence their structure^{38,39}. The artificial microbiotas, AM1 and AM2,
303 follow similar trends as the *A. baylyi* and they come even closer to *A. baylyi* after
304 extended exposure to the kanamycin antibiotic. After PCA-LDA, the most
305 discriminating peaks were observed in Gram-negative bacteria and were attributed to
306 lipids ($\sim 1750\text{ cm}^{-1}$), $\nu_{\text{as}}\text{PO}_2^-$ ($\sim 1225\text{ cm}^{-1}$) and $\nu_{\text{s}}\text{PO}_2^-$ ($\sim 1080\text{ cm}^{-1}$). Kanamycin's
307 antimicrobial mechanism is associated with aminoglycosides, interfering with
308 aminoacyl-tRNA recognition at the ribosomal A site and disrupting protein
309 expression⁴⁰. Such a mechanism causes series of secondary effects, *e.g.*, membrane
310 damage. Our results are consistent with previous findings showing that the damage is
311 mainly linked to a broad range of alterations associated with the elements of
312 membranes, *e.g.*, proteins, supported by derived peaks the protein absorbance region
313 from $1500\text{ to }1700\text{ cm}^{-1}$, such as Amide II ($\sim 1517\text{ cm}^{-1}$, $\sim 1543\text{ cm}^{-1}$) and Amide I

314 ($\sim 1650\text{ cm}^{-1}$, $\sim 1680\text{ cm}^{-1}$)^{16,21,41,42}.

315 Applying the linear D_t regression model, we successfully predicted the dynamic
316 abundance of *A. baylyi* and kanamycin resistance within the microbiotas under
317 kanamycin antibiotic pressures. Both artificial microbiotas, AM1 (Figure 4B) and
318 AM2 (Figure 4C), had defined community composition at 0 h, with *A. baylyi*
319 (kanamycin resistance gene) accounting for 10% and 40% of the total population,
320 respectively. Post-exposure to kanamycin, the ARGs abundance from qPCR results
321 gradually increased to 85.0% in AM1 and 92.2% in AM2 after 12 h, which is
322 explained by the competitive advantages of bacteria with kanamycin resistance gene
323 in the community⁴³. It therefore led to a faster growth of *A. baylyi* compared to other
324 strains and subsequent dominance of *A. baylyi* within the microbiota. From the
325 dynamics of discriminant functions, the predicted ARGs abundance in both
326 microbiotas fitted efficiently with experimental data (Figure 4B and 4C). The linear
327 correlation at each time point did not show significant difference between predicted
328 and experimental ARGs abundance (Figure 4D), with a Pearson correlation
329 coefficient of 0.9487. The prediction *via* infrared spectroscopy coupled and
330 multivariate analysis fitted the experimental data better at higher ARGs abundance,
331 but was slightly lower than the qPCR results at low ARGs abundance, *e.g.*, 33% in
332 Figure 4D, which might underestimate the ARGs abundance to some extent. These
333 results not only prove that our model can be used for static community composition
334 and abundance/dynamics of kanamycin resistance gene, but they also evaluate the
335 impact of antibiotic pressure on kanamycin resistance gene transfer or dominance.

336



337

338 **Figure 4.** (A) Two-dimensional (LD1, LD2) scores plot after PCA-LDA of IR
339 dynamics of artificial microbiotas. Dots along with the arrow point in each colour

340 refer to the measurement at 0, 4, 8, 12 and 24 h, respectively. The prediction of
341 kanamycin resistance gene abundance is based on the dispersion among the
342 classification groups in PCA-LDA for artificial microbiotas AM1 (B) and AM2 (C).
343 (D) Regression correlation of kanamycin resistance gene abundance between
344 experimental data *via* qPCR and model prediction.

345

346 It is worth mentioning that less dispersion is observed for *A. baylyi* after exposure
347 because *A. baylyi* ADPWH_recA contains the *kan^R* kanamycin resistance gene, which
348 is capable of tolerating kanamycin pressure. In the present study, the *kan^R* kanamycin
349 resistance gene belongs to *npt* encoding neomycin phosphotransferase and shows high
350 similarity to *addA* encoding aminoglycoside phosphotransferase (aminoglycoside
351 kinase), which modifies the aminoglycosides by phosphoryl transfer, catalysing the
352 phosphate addition from ATP to 3'-hydroxyl group⁴⁰. By expressing *kan^R*, *A. baylyi*
353 ADPWH_recA inactivates the interference of protein expression by kanamycin,
354 achieves fast recovery from suppression, and minimizes spectral alterations as
355 compared to others. It is confirmed by the presence of consistent shifts and
356 discriminating biomarkers in *A. baylyi* postexposure to kanamycin, including Amide I
357 ($\sim 1630\text{ cm}^{-1}$, $\sim 1640\text{ cm}^{-1}$) and $\nu_{\text{as}}\text{PO}_2^-$ ($\sim 1222\text{ cm}^{-1}$, $\sim 1235\text{ cm}^{-1}$)⁴².

358 An unexpected decline of kanamycin resistance gene was observed for AM2
359 artificial microbiota after 24 h exposure to kanamycin (42%, Figure 4C), but the
360 predicted kanamycin resistance by D_I regression model remained close to 100%. It
361 might be explained by the dramatically decreasing kanamycin concentration via the
362 metabolism of aminoglycoside modifying enzyme and the change in microbial
363 community structure. The functions of *kan^R* encoding aminoglycoside kinase are
364 stabilizing a metaphosphate transition state and inactivating kanamycin³¹, and the
365 spectral alterations represent the alignment disruption of β -phosphate and γ -phosphate
366 by amide backbone. The declining kanamycin results in less inhibition on bacteria
367 without kanamycin resistance gene (*M. vanbaalenii* and *E. coli*), and their growth and
368 regeneration consequently reduce the abundance of *A. baylyi* and *kan^R* gene.
369 Alternatively, the FTIR spectral alteration reflects such phenotypic changes of the
370 whole microbiota under the low kanamycin exposure, illustrating the fact that the
371 majority of microbial cells within the microbiota have the pseudo-resistance to

372 kanamycin. The spectrochemical interrogation therefore actually quantifies the
373 microbial phenotypic antibiotic resistance rather than the ARGs abundance only.

374 Infrared spectroscopy has demonstrated the ability to diagnose the phenotypic
375 alteration of the cellular components induced by kanamycin, hinting its potential
376 possibility for the application to other members of the aminoglycoside family. Our
377 findings indicate that this dispersion model coupled with PCA-LDA is a potential
378 approach for monitoring the population dynamics within a microbiota in real-time.
379 Additionally, the model applied in the present study summarizes the whole spectral
380 information derived from the multivariate analysis, rather than only several
381 biomarkers, showing its potential as a universal predicting tool for a broad spectrum
382 of antibiotics based on well-trained databases. Though only successfully applied in
383 the case of kanamycin through phosphotransferase resistance pathway, this technique
384 is also feasible for detecting *N*-acetyltransferases and *O*-nucleotidyltransferases,
385 which also belong to aminoglycoside-modifying enzymes assisted by
386 acetyl-coenzyme A and ATP respectively²², attributing to their similar anti-kanamycin
387 mechanisms as *kan^R* encoding neomycin phosphotransferase. Future work should
388 refer to more comprehensive range of antibiotics and their mechanisms including
389 penicillin-class (*e.g.*, ampicillin and amoxicillin), which disrupts the synthesis of
390 peptidoglycan layer and inhibits bacterial cell wall synthesis⁴⁴, and tetracycline,
391 which inhibits the binding of aminoacyl-tRNA and suppresses protein expression⁴⁵.
392 For the urgent need to characterize antibiotic resistance in complex environmental
393 microbiota with spectroscopy, the primary challenges are raised as the lack of routine
394 protocols, reproducible computational analysis, and reliable database¹⁰. Validated in
395 the artificial microbiota, our work provides the solutions for the first two barriers by
396 distinguishing biomarkers representing antibiotic resistance from the numerous
397 biological fingerprints. A well-built dataset along with robust analytical models
398 coupled with spectroscopic methods are suggested to address the antibiotic resistance
399 dynamics in real environmental samples.

400 The present study indicates that infrared spectroscopy, in conjunction with
401 multivariate analysis, is a potential tool for diagnosing the phenotypic existence and
402 dynamics of ARGs within microbial communities. Our work employed ATR-FTIR
403 spectroscopy coupled with a dispersion model to quantify microbial kanamycin
404 resistance, based on secondary derivative and PCA-LDA. This method not only

405 quantified the static community composition of the artificial microbiotas but also
406 successfully predicted the population dynamics of microbial communities and
407 kanamycin resistance under antibiotic pressure. We also suggest that spectroscopic
408 techniques have great potential in real-time monitoring of microbiota of interest in
409 medical or environmental fields; this would provide an excellent opportunity to
410 visualize the vivid phenotypic transformation during a biological and biochemical
411 process rather than only intermittent snap-shots.

412

413 **Acknowledgements** N.J. was funded by Chinese Academy of Sciences and China
414 Scholarship Council. Research is supported by the Engineering and Physical Sciences
415 Research Council in F.L.M.'s laboratory (EPSRC; grant no: EP/K023349/1) and
416 National Natural Science Foundation of China in D.Z.'s laboratory (NFSC; grant no:
417 41301331).

418

419

420 **References**

- 421 (1) Blair, J. M.; Webber, M. A.; Baylay, A. J.; Ogbolu, D. O.; Piddock, L. J. *Nat. Rev.*
422 *Microbiol.* **2015**, *13*, 42-51.
- 423 (2) Chee-Sanford, J. C.; Aminov, R. I.; Krapac, I. J.; Garrigues-Jeanjean, N.; Mackie,
424 R. I. *Appl. Environ. Microbiol.* **2001**, *67*, 1494-1502.
- 425 (3) Cantas, L.; Shah, S. Q. A.; Cavaco, L. M.; Manaia, C. M.; Walsh, F.; Popowska,
426 M.; Garelick, H.; Burgmann, H.; Sorum, H. *Front. Microbiol.* **2013**, *4*.
- 427 (4) Potera, C. *Environ. Health Perspect.* **2013**, *121*, A255-A255.
- 428 (5) Smillie, C. S.; Smith, M. B.; Friedman, J.; Cordero, O. X.; David, L. A.; Alm, E. J.
429 *Nature* **2011**, *480*, 241-244.
- 430 (6) Colomer-Lluch, M.; Imamovic, L.; Jofre, J.; Muniesa, M. *Antimicrob. Agents*
431 *Chemother.* **2011**, *55*, 4908-4911.
- 432 (7) Riesenfeld, C. S.; Goodman, R. M.; Handelsman, J. *Environ. Microbiol.* **2004**, *6*,
433 981-989.
- 434 (8) Paraskevaidi, M.; Martin-Hirsch, P. L.; Kyrgiou, M.; Martin, F. L. *Mutagenesis*
435 **2017**, *32*, 335-342.
- 436 (9) Kaern, M.; Elston, T. C.; Blake, W. J.; Collins, J. J. *Nat. Rev. Genet.* **2005**, *6*,
437 451-464.
- 438 (10) Jin, N. F.; Zhang, D. Y.; Martin, F. L. *Integr. Biol.* **2017**, *9*, 406-417.
- 439 (11) Naumann, D.; Helm, D.; Labischinski, H. *Nature* **1991**, *351*, 81-82.
- 440 (12) Dunn, W. B.; Ellis, D. I. *Trends Anal. Chem.* **2005**, *24*, 285-294.
- 441 (13) Freedman, B. G.; Zu, T. N. K.; Wallace, R. S.; Senger, R. S. *Biotechnol. J.* **2016**,
442 *11*, 877-889.
- 443 (14) Sun, S. W.; Wang, X. T.; Gao, X.; Ren, L. H.; Su, X. Q.; Bu, D. B.; Ning, K.
444 *BMC Bioinformatics* **2015**, *16*.
- 445 (15) Winnard, P. T.; Zhang, C.; Vesuna, F.; Kang, J. W.; Garry, J.; Dasari, R. R.;
446 Barman, I.; Raman, V. *Oncotarget* **2017**, *8*, 20266-20287.
- 447 (16) Li, J. Y.; Strong, R.; Trevisan, J.; Fogarty, S. W.; Fullwood, N. J.; Jones, K. C.;
448 Martin, F. L. *Environ. Sci. Technol.* **2013**, *47*, 10005-10011.

449 (17) Bankapur, A.; Krishnamurthy, R. S.; Zachariah, E.; Santhosh, C.; Chougule, B.;
450 Praveen, B.; Valiathan, M.; Mathur, D. *PLoS One* **2012**, *7*.

451 (18) Tao, Y. F.; Wang, Y.; Huang, S.; Zhu, P. F.; Huang, W. E.; Ling, J. Q.; Xu, J.
452 *Anal. Chem.* **2017**, *89*, 4108-4115.

453 (19) Siddhanta, S.; Paidi, S. K.; Bushley, K.; Prasad, R.; Barman, I. *Chemphyschem*
454 **2017**, *18*, 72-78.

455 (20) Baker, M. J.; Trevisan, J.; Bassan, P.; Bhargava, R.; Butler, H. J.; Dorling, K. M.;
456 Fielden, P. R.; Fogarty, S. W.; Fullwood, N. J.; Heys, K. A.; Hughes, C.; Lasch, P.;
457 Martin-Hirsch, P. L.; Obinaju, B.; Sockalingum, G. D.; Sule-Suso, J.; Strong, R. J.;
458 Walsh, M. J.; Wood, B. R.; Gardner, P.; Martin, F. L. *Nat. Protoc.* **2014**, *9*,
459 1771-1791.

460 (21) Martin, F. L.; Kelly, J. G.; Llabjani, V.; Martin-Hirsch, P. L.; Patel, II; Trevisan,
461 J.; Fullwood, N. J.; Walsh, M. J. *Nat. Protoc.* **2010**, *5*, 1748-1760.

462 (22) Mingeot-Leclercq, M. P.; Glupczynski, Y.; Tulkens, P. M. *Antimicrob. Agents*
463 *Chemother.* **1999**, *43*, 727-737.

464 (23) Sadovskaya, I.; Vinogradov, E.; Li, J. J.; Hachani, A.; Kowalska, K.; Filloux, A.
465 *Glycobiology* **2010**, *20*, 895-904.

466 (24) Delorenzo, V.; Herrero, M.; Jakubzik, U.; Timmis, K. N. *J. Bacteriol.* **1990**, *172*,
467 6568-6572.

468 (25) Song, Y.; Li, G.; Thornton, S. F.; Thompson, I. P.; Banwart, S. A.; Lerner, D. N.;
469 Huang, W. E. *Environ. Sci. Technol.* **2009**, *43*, 7931-7938.

470 (26) Trevisan, J.; Angelov, P. P.; Scott, A. D.; Carmichael, P. L.; Martin, F. L.
471 *Bioinformatics* **2013**, *29*, 1095-1097.

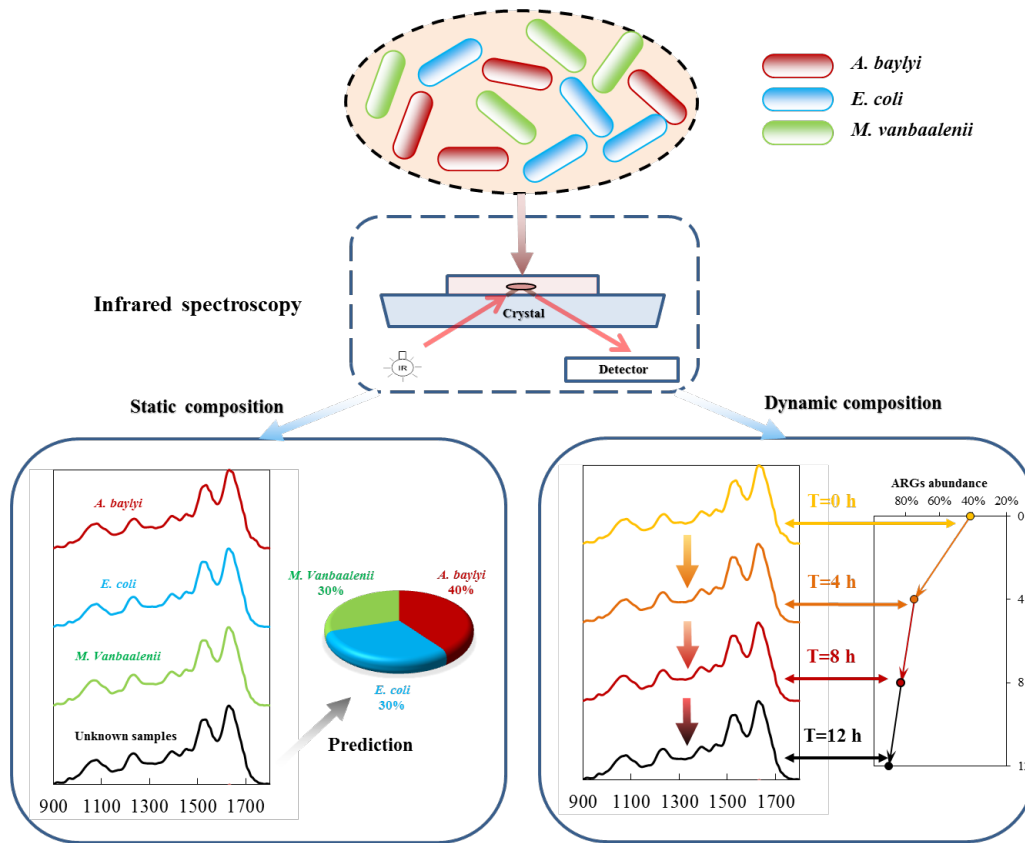
472 (27) Butler, H. J.; McAinsh, M. R.; Adams, S.; Martin, F. L. *Anal. Methods* **2015**, *7*,
473 4059-4070.

474 (28) Yenofsky, R. L.; Fine, M.; Pellow, J. W. *Proc. Natl. Acad. Sci. U. S. A.* **1990**, *87*,
475 3435-3439.

476 (29) Bosch, A.; Serra, D.; Prieto, C.; Schmitt, J.; Naumann, D.; Yantorno, O. *Appl.*
477 *Microbiol. Biotechnol.* **2006**, *71*, 736-747.

- 478 (30) Mariey, L.; Signolle, J. P.; Amiel, C.; Travert, J. *Vib. Spectrosc.* **2001**, *26*,
479 151-159.
- 480 (31) Wright, G. D. *Curr. Opin. Microbiol.* **1999**, *2*, 499-503.
- 481 (32) Flemming, H. C.; Wingender, J. *Nat. Rev. Microbiol.* **2010**, *8*, 623-633.
- 482 (33) Holman, H. Y. N.; Miles, R.; Hao, Z.; Wozzi, E.; Anderson, L. M.; Yang, H.
483 *Anal. Chem.* **2009**, *81*, 8564-8570.
- 484 (34) Stewart, P. S. *Int. J. Med. Microbiol.* **2002**, *292*, 107-113.
- 485 (35) Hoiby, N.; Bjarnsholt, T.; Givskov, M.; Molin, S.; Ciofu, O. *Int. J. Antimicrob.*
486 *Agents* **2010**, *35*, 322-332.
- 487 (36) Karunakaran, E.; Mukherjee, J.; Ramalingam, B.; Biggs, C. A. *Appl. Microbiol.*
488 *Biotechnol.* **2011**, *90*, 1869-1881.
- 489 (37) Li, H. B.; Martin, F. L.; Zhang, D. Y. *Anal. Chem.* **2017**, *89*, 3909-3918.
- 490 (38) Ede, S. M.; Hafner, L. M.; Fredericks, P. M. *Appl. Spectrosc.* **2004**, *58*, 317-322.
- 491 (39) Morones, J. R.; Elechiguerra, J. L.; Camacho, A.; Holt, K.; Kouri, J. B.; Ramirez,
492 J. T.; Yacaman, M. J. *Nanotechnology* **2005**, *16*, 2346-2353.
- 493 (40) Boehr, D. D.; Thompson, P. R.; Wright, G. D. *J. Biol. Chem.* **2001**, *276*,
494 23929-23936.
- 495 (41) Heys, K. A.; Riding, M. J.; Strong, R. J.; Shore, R. F.; Pereira, M. G.; Jones, K.
496 C.; Semple, K. T.; Martin, F. L. *Analyst* **2014**, *139*, 896-905.
- 497 (42) Movasaghi, Z.; Rehman, S.; Rehman, I. U. *Appl. Spectrosc. Rev.* **2008**, *43*,
498 134-179.
- 499 (43) Hibbing, M. E.; Fuqua, C.; Parsek, M. R.; Peterson, S. B. *Nat. Rev. Microbiol.*
500 **2010**, *8*, 15-25.
- 501 (44) Strominger, J. L.; Park, J. T.; Thompson, R. E. *J. Biol. Chem.* **1959**, *234*,
502 3263-3268.
- 503 (45) Connell, S. R.; Trieber, C. A.; Dinos, G. P.; Einfeldt, E.; Taylor, D. E.; Nierhaus,
504 K. H. *EMBO J.* **2003**, *22*, 945-953.
- 505
- 506

Table of Content Graphic



508

509

510

511

512

For TOC only